Measurement of Droplet Interfacial Phenomena by Light-Scattering Techniques

Two light-scattering techniques have been applied to study the kinetics of droplet evaporation and attendant interfacial phenomena. The first technique, which is particularly useful for noisy data, utilizes the fast Fourier transform of phase function data (intensity vs. scattering angle) to obtain the size by comparing the phase function with Lorenz-Mie theory. The second method applies optical resonance measurements to obtain very precise measurements of size and/or refractive index as functions of time. The techniques have been used to measure the slow evaporation of multicomponent and single-component organic microdroplets, rapid evaporation of water droplets, and rapid evaporation of droplets of aqueous solutions and surfactant solutions. The experiments were performed in an electrodynamic balance, which was used to suspend single microdroplets in a polarized laser beam. Rapid evaporation rate data yield information on the surface temperature, and data for surfactant solution evaporation show that insoluble monolayer formation at the microdroplet surface reduces the evaporation rate by a factor of 200. In addition, it is shown that droplet explosion due to surface charge effects can occur well below the Rayleigh limit of charge.

Daniel C. Taflin, S. H. Zhang, Theresa Allen, E. James Davis
Department of Chemical Engineering
University of Washington
Seattle, WA 98195

Introduction

Rates of spray drying, droplet combustion, and numerous other processes involving volatile droplets are often controlled by evaporation of the volatile species. Rapid evaporation of agricultural sprays, such as aqueous solutions of pesticides, can cause the droplets to drift before they fall to earth because of their decreasing terminal velocities. Rate measurements *in situ* are not easily made in the atmosphere and in industrial equipment, and until recently rapid evaporation measurements under carefully controlled conditions that simulate applications were difficult to perform in the laboratory. The development of the electrodynamic balance, which uses superposed a.c. and d.c. electrical fields to suspend a small charged droplet (0.1–200 μm diam.) in a flow field and/or in a laser beam, has made it possible to study a wide variety of phenomena, indicated by the review of Davis (1987b).

A major advantage of the electrodynamic balance for microdroplet measurements is that optical methods can be used for extremely precise measurement of size, but for volatile materials measurements of evaporation and condensation must be made very rapidly. In the studies cited by Davis rapid evaporation was either not encountered or it was not necessary to determine rates of size change. Furthermore, most of the techniques used to date for size measurement cannot be applied when rapid changes are involved, for the response time of the instrumentation is too slow. This paper addresses the problem of measuring rapid evaporation rates of microdroplets.

The conventional light-scattering methods used to size colloidal particles and aerosols are:

1. Measurement of the polarization ratio (ratio of scattered intensities using vertically and horizontally polarized laser light) at one or more angles
2. Measurement of the phase function (scattered intensity vs. angle)

Single angle measurements can be made very rapidly, but if neither the refractive index nor the size of the microscope is known, the interpretation of the polarization ratio to obtain size and/or refractive index can be ambiguous. Phase function data provide us with a precise method of determining size and refractive index of microspheres (Davis and Periasamy, 1985), but many data points are needed to permit unambiguous comparison of the experimental phase function with that computed using Lorenz-Mie theory (Lorenz, 1890; Mie, 1908). Using electrostatic balances, Gucker and Egan (1961) and Wyatt and Phillips (1972) obtained phase function data by means of a

rotating photomultiplier tube (PMT), which was used to record the intensity of scattered light through a window in a Millikan-like chamber. Davis and Ray (1980) used this same technique with their electrodynamic balance, but the time required to obtain the phase function over an angle range of 160° was several seconds. For rapidly changing microdroplets this is much too slow, so alternate techniques are required to study the dynamics of microparticles. Davis (1987a) and Pluchino (1987) replaced the rotating PMT with photodiode arrays to record the phase function nearly instantaneously. Davis used a 512-element linear photodiode array, and Pluchino used 64 photodetectors.

An alternate, and more recently developed, procedure for obtaining very precise size information for microdroplets involves optical resonance measurements. Optical resonances or structural resonances are the natural modes of oscillation of a dielectric medium when illuminated by a source of electromagnetic radiation. Since Ashkin and Dziedzic (1977) first recognized the utility of resonant light scattering for measuring the optical properties of microparticles, a number of laboratories have applied the principles to study evaporation and growth (Richardson et al., 1986a, b; Taflin and Davis, 1987), and Tzeng et al. (1984) measured evaporation and condensation rates of liquid droplets using resonances in fluorescence spectra. Numerous theoretical studies of resonance structures have been published, such as those of Chylek et al. (1978, 1983), Barber et al. (1982), and Conwell et al. (1984).

A brief overview of Lorenz-Mie theory is in order to permit interpretation of light-scattering data. For a sphere of radius a and refractive index m illuminated with a vertically polarized laser beam with wavelength λ, the intensity of the light scattered in the horizontal plane is given by

$$I_1 = \left\{ \sum_{n=1}^{\infty} \frac{2n+1}{n(n+1)} \left[a_n \frac{P_n^1(\cos\theta)}{\sin\theta} + b_n \frac{d}{d\theta} P_n^1(\cos\theta) \right] \right\}^2 \quad (1)$$

where $P_n^1(\cos\theta)$ is the associated Legendre function, and θ is the scattering angle measured from the back side of the sphere.

Resonances correspond to zeros of the denominators of the coefficients a_n and b_n, where a_n and b_n are functions of the optical size α ($\alpha = 2\pi a/\lambda$) and the refractive index given by

$$a_n = \frac{j_n(\alpha)[m\alpha j_n(m\alpha)]' - m^2 j_n(m\alpha)[\alpha j_n(\alpha)]'}{h_n^{(2)}(\alpha)[m\alpha j_n(m\alpha)]' - m^2 j_n(m\alpha)[\alpha h_n^{(2)}(\alpha)]'} \quad (2)$$

and

$$b_n = \frac{j_n(\alpha)[m\alpha j_n(m\alpha)]' - j_n(m\alpha)[\alpha j_n(\alpha)]'}{h_n^{(2)}(\alpha)[m\alpha j_n(m\alpha)]' - j_n(m\alpha)[\alpha h_n^{(2)}(\alpha)]'} \quad (3)$$

Although the phase function (intensity vs. scattering angle θ) is highly sensitive to size and moderately sensitive to refractive index, the resonance spectrum is much more sensitive to each of these parameters. Chylek et al. (1983) showed that the droplet size and refractive index can be determined with the relative errors $\Delta\alpha/\alpha = 4 \times 10^{-5}$ and $\Delta m/m = 4 \times 10^{-5}$. This remarkable sensitivity to size is the basis of the measurement of infrared absorption spectra of microdroplets developed by Arnold and coworkers (1982, 1985), who illuminated the microdroplet with a narrow band of IR radiation to produce a small amount of evaporation. The intensity increase associated with a resonance was then used to measure the decrease in α, which was proportional to the IR absorption.

It is the purpose of this paper to show that resonance measurements and high-speed phase function measurements can be used to examine interfacial properties of evaporating droplets as well as evaporation rates.

Mass Transfer Theory

For a relatively nonvolatile droplet the evaporation rate in the continuum regime proceeds very nearly isothermally (Chang and Davis, 1974), and, based on the quasisteady-state assumption, the mass flux at the droplet surface ($r = a$) for evaporation of pure-component species i into a stagnant, vapor-free carrier gas j is given by

$$J_a = -D_{ij} p_i^o M_i / aRT_a \quad (4)$$

where the interfacial temperature T_a is very nearly equal to the bulk gas temperature T_∞, and the vapor pressure p_i^o is evaluated at the interfacial temperature.

For rapid evaporation three complicating factors arise; Wagner (1982) has reviewed the theory and principles involved. In this case the latent heat of vaporization must be supplied by heat transfer from the gas and liquid phases, primarily from the gas phase (Chang and Davis, 1974), so the heat and mass transport processes are coupled. The complicating factors are Stefan flow (the convective flow associated with vapor transport from the surface), thermal diffusion, and the thermal energy of the diffusing species. A higher order quasisteady-state solution leads to the following energy balance between the net heat transferred from the gas phase and the latent heat transferred by the diffusing species:

$$k_j \phi_H (T_\infty - T_a) = \lambda_i D_{ij} \phi_M p_i^o M_i / RT_a \quad (5)$$

where ϕ_H and ϕ_M are heat and mass transfer correction factors, respectively, defined by

$$\phi_H = 1 - \frac{1}{2\lambda_i}\left[\frac{R\alpha_T}{M_i}(T_\infty + T_a) + C_{pj}(T_a - T_\infty)\right] + \frac{D_{ij} p_i^o (1+\alpha_T)}{2k_j RT_a}\left[\alpha_T + C_{pj}\frac{(T_a - T_\infty)}{RT_a}\right] \quad (6)$$

and

$$\phi_M = \frac{1}{2}\left[1 + \frac{1 - \lambda_i D_{ij} p_i^o (1+\alpha_T)/k_j RT_a^2}{(1 - p_i^o/P)}\right] \quad (7)$$

The thermal diffusion factor α_T has not been determined reliably, but Katz and Mirabel (1975) suggested that $\alpha_T = 0.01$ for water vapor and air. For the systems considered in this study ϕ_H and ϕ_M are nearly unity and are not affected by the value of α_T used in the calculations. That is, thermal diffusion is not significant.

Now Eq. 4 can be solved to determine the interfacial temperature, and the rate of change of droplet radius with time can be obtained by material balance on the droplet to give:

$$J_a = -\frac{1}{4\pi a^2}\frac{d}{dt}\left(p_L \frac{4}{3}\pi a^3\right) = \frac{D_{ij}}{a}\phi_M \frac{p_i^o M_i}{RT_a} \quad (8)$$

which, for constant T_a, can be integrated with respect to time to yield:

$$a^2 = a_o^2 - (2D_{ij}\phi_M p_i^o M_i/\rho_L R T_a)t \qquad (9)$$

From Eq. 9 a plot of measured values of a^2 vs. t should yield a straight line with slope $S_{ij} = -2D_{ij}\phi_M p_i^o M_i/\rho_L R T_a$, and the interfacial temperature can be determined from the measured slope provided that D_{ij} and p_i^o are known as functions of temperature.

If the surrounding gas is not stagnant, convective mass transfer must be taken into account, as discussed by Zhang and Davis (1987), but for small Peclet numbers ($Pe \ll 1$, where $Pe = 2av/D_{ij}$, and v is the gas velocity) the correction to Eq. 9 is insignificant. For the microdroplet radii and gas velocities encountered in this study the assumption of a stagnant surrounding medium is valid.

For a multicomponent droplet several complications arise. The interfacial partial pressures of the evaporating species vary as the droplet composition changes due to loss of the more volatile components. This distillation effect will cause the evaporation rate to decrease with time. When a slightly soluble nonvolatile component is involved, crystallization can occur as solvent evaporates. Furthermore, if one component is surface-active, the formation of an insoluble monolayer at the interface can reduce the evaporation rate by introducing an interfacial resistance to mass transfer. Frey and King (1986) showed that surfactants can have a substantial effect on mass transfer in spray drying. All of these complications will be examined herein.

Experimental Techniques

Two electrodynamic balances (picobalances), which had the same electrode configurations but different optical components, were used in this study. One of the devices has been described in some detail by Davis (1987a), so only a brief description of the newer instrument is sufficient here. The picobalance shown in Figure 1 was used to suspend a single charged droplet in a vertically polarized laser beam by means of superposed a.c. and d.c. electrical fields. The a.c. field focuses the microdroplet in the center of the chamber, and the d.c. field is used to balance gravitational, aerodynamic, and other vertical forces. The bihyperboloidal electrode configuration of Wuerker et al. (1959) was used

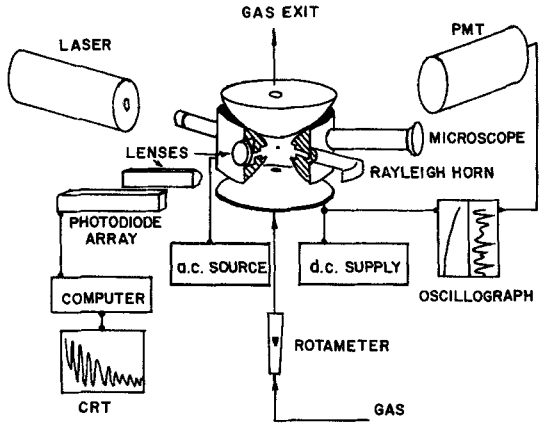

Figure 1. Electrodynamic balance and peripheral equipment used for experiments.

for both balances, but for the new balance a trough was cut in the a.c. electrode to eliminate asymmetries associated with the holes and window in the ring electrode. The droplet could be maintained at the null point of the balance either by manual control (only manual control in the newer device) of the d.c. voltage or by means of a PID controller that operated on signals from a dual photodiode detector (ASE Pid) used to detect forward-scattered light collected by a lens mounted in the ring electrode. The electrooptic controller applied a control potential to the upper electrode, and the potential of the lower electrode could be set independently within the range ±320 V.

A 512-element linear photodiode array (Reticon 512EC/17) was used to detect and record forward-scattered light in the range $34° \leq \theta \leq 71°$. In one balance the array was mounted directly over a window in the ring electrode, and in the other a cylindrical lens was used to focus a narrow horizontal slit of light on the array, which could then be moved away from the a.c. electrode to permit the array to be cooled for future applications. Multiplex switches, driven by an external clock, provided sequential readout of the light level from each of the 512 pixels at a rate of 80 μs per pixel; this output was sent to a high-frequency analog/digital converter (Data Translation 3382) and recorded using a digital computer (Digital Equipment Corp. MINC 23). Thus, a single scan of the 512 pixels required less than about 40 ms, so it was possible to obtain numerous "phase functions" over a short period of time. To control and set the timing sequence for recording these phase function data a pulse-counting logic circuit was used. This permitted us to sample the data at an adjustable rate ranging from 4 to 300 scans per minute. For lower rates there was sufficient time to dump the buffer and store the data on floppy disks after each scan, but for the most rapid data acquisition the size of the buffer in the computer limited us to 10 scans. After 10 automatic scans were obtained, we switched to scan-on-demand.

An additional feature of the balance was that a metered flow of gas could be passed through the chamber by means of holes drilled through the centers of the top and bottom electrodes. The gas, usually nitrogen, was dried, passed through a constant-temperature bath, metered with a calibrated rotameter, and introduced into the chamber as a laminar jet. It was essential to flow gas through the balance in order to remove vapor produced by droplet evaporation and prevent partial saturation of the gas phase. The gas could also be humidified prior to entering the balance to provide a controlled-humidity environment.

Droplets were generated and charged in either of two ways:

1. By suddenly charging either a hypodermic needle or a solid metal rod with a cavity in the end
2. By means of a piezoelectric tube crystal with a small orifice attached to its lower end and a charging ring mounted below it

A d.c. voltage of the order of 5,000 V was applied to the needle or rod by means of a high-voltage relay (Magnecraft 10 kV reed relay). By this procedure the electrical stress produced at the liquid surface opposes the surface tension, a charged microdroplet is formed, and it falls into the balance chamber through the hole in the top electrode. Using the piezoelectric crystal, a d.c. pulse was applied to the outer surface of the tube to generate a microdroplet at the orifice, and a d.c. voltage of order 1,000 V was applied to the charging ring to inductively charge the droplet. The a.c. and d.c. fields of the balance were present to trap the particle, and the d.c. voltage was quickly adjusted to balance

the particle in the laser beam. At the same time that the high voltage was applied to the needle, or to the piezoelectric crystal, a start pulse was generated to initiate the data acquisition system to record the phase function data. For the rapid evaporation rates of particular interest here it is essential that the d.c. voltage be adjusted manually to balance the particle within 1 s, a challenging task.

Phase functions

A typical output of the linear photodiode array is shown in Figure 2, which is for a droplet of sodium dodecyl sulfate (SDS) in water evaporating into dry nitrogen at 20°C. The three scans shown represent the seventh, eighth, and tenth of a set with a scan rate of approximately one scan per second. We note that both the intensity of the scattered light and the number of peaks changed significantly as the droplet evaporated. For the size range shown, the number of peaks in the angle range covered is directly proportional to the droplet diameter, but for smaller microdroplets ($\alpha < 10$) the size can be determined by comparing the measured phase function with predictions from Mie theory.

We also note that for angles greater than 60° there is considerable noise identifiable in the phase function data. For very small droplets the phase function data are very noisy, and additional processing of the data is required. Numerous sources of noise affect phase function data obtained with photodiode arrays; these include thermal noise associated with thermionic emission in the photodiodes, variations in the quantum efficiency from pixel to pixel, and fluctuations in the intensity of the laser light source. Thermal noise can be reduced by cooling the array, and the new design of the mounting system was carried out to permit the array to be cooled, although it was not cooled in this study. Variations in quantum efficiency can be taken into account by calibration of the array, but we have processed noisy data by applying a fast Fourier transform (FFT) algorithm of Bergland (1969). As the application of FFT to phase function data is novel, some details are in order.

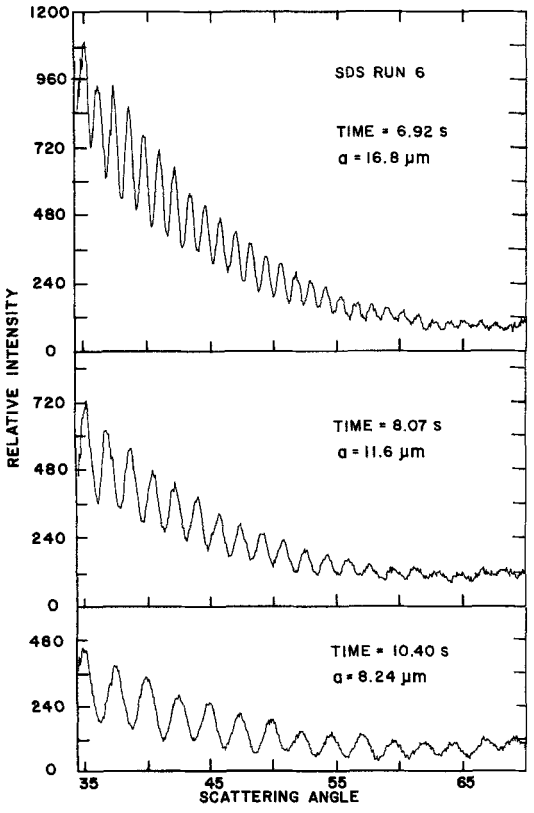

Figure 2. Output of photodiode array for a droplet of sodium dodecyl sulfate in water evaporating in dry nitrogen at 293 K.

FFT data processing

Let $I_k^* = I^*(x_k)$ be the measured intensity of the kth pixel, which is located at distance x_k measured from the center of the linear array. If x_{max} is the distance from the center to the last pixel, then x_k is related to x_{max} by

$$x_k = [2k/(N-1) - 1]x_{max} \tag{10}$$

where N is the number of pixels (usually 512), and k varies from 0 to $N-1$.

Now I_k^* must be corrected for parallax because the photodiode array is flat and does not follow the curvature of the ring electrode. An additional correction must be made because the photodiode elements farther from the middle of the array are farther from the light-scattering source. The corrected intensity, then, is given by

$$I_k = I_k^*\left\{1 + \left[\left(\frac{2k}{N-1} - 1\right)\tan\theta_{max}\right]^2\right\}^{3/2} \tag{11}$$

where θ_{max} is the angle corresponding to the edge of the array.

The representation of the corrected intensity (a real variable) for equally spaced points x_k is given by

$$I_k = A_o + (-1)^k A_{N/2} + 2\sum_{j=1}^{N/2-1} Re\left[A_j \exp\left(-\frac{2\pi ijk}{N}\right)\right] \tag{12}$$

where $i = \sqrt{-1}$ here, and j and k are indices. The amplitudes A_j are obtained from the following equation, the discrete Fourier transform of I_k,

$$A_j = \frac{1}{N}\sum_{k=0}^{N-1} I_k \exp\left(\frac{2\pi ijk}{N}\right) \tag{13}$$

Now Eq. 12, which is a representation of the intensities corresponding to equally spaced points in x, can be used to generate a vector, J_k, of equally spaced points in θ, where x and θ are related by

$$x = D\tan\theta \tag{14}$$

and D is the distance between the microdroplet and the center of the photodiode array. This was accomplished by letting k be continuous and resampling $I(x_k)$ at points corresponding to equal spacing in θ. Next, J_k is transformed to yield a new amplitude vector, B_j, which has the same form as Eq. 13 with I_k replaced by J_k. To eliminate the high-frequency noise we set all amplitudes B_j to zero for $j > j_{cutoff}$. This cutoff frequency can be selected by examining B_j as a function of frequency, j. As we

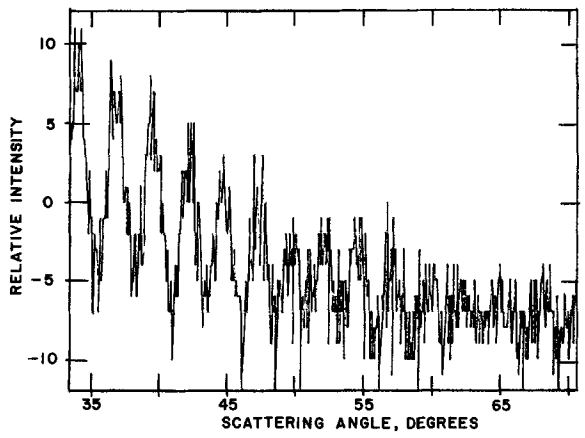

Figure 3. Noisy data from photodiode array obtained with a low-intensity helium-neon laser.

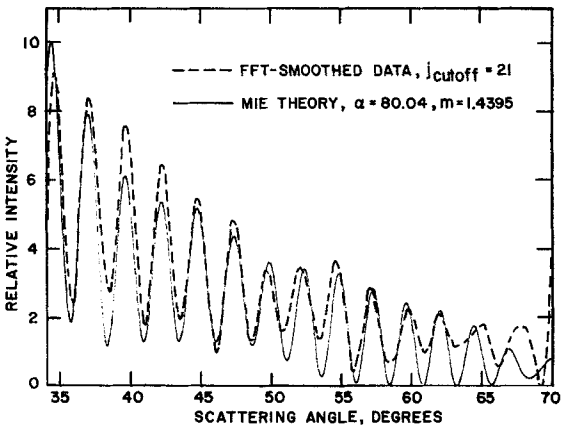

Figure 5. Smoothed data of Figure 3 compared with Mie theory.

shall show, there is a well-defined maximum frequency in the "power spectrum," P_j, and frequencies above this maximum can be eliminated. The power spectrum is defined by

$$P_j = [(B_{j,Re})^2 + (B_{j,Im})^2]^{1/2} \tag{15}$$

where $B_{j,Re}$ and $B_{j,Im}$ are the real and imaginary components of the complex numbers B_j, respectively.

This FFT processing of noisy phase function data is illustrated in Figures 3 through 5, which show results for dodecanol evaporating in air at room temperature, using a helium-neon laser (λ = 632.8 nm). Figure 3 shows the output of the photodiode array as a function of angle θ; the data are particularly noisy for $\theta > 50°$. Figure 4 shows the real and imaginary components of the amplitudes A_j and the power spectrum obtained by the forward transformation of the intensities of Figure 3. The power spectrum shows a well-defined peak at $j = 14$. If we use a cutoff frequency of $j_{cutoff} = 21$ and apply the inverse transformation, we obtain the phase function shown as the dashed line in Figure 5. Also shown in Figure 5 as a solid line is the theoretical phase function computed from Mie theory for $\alpha = 80.04$ ($a = 8.061$ μm) and $m = 1.4395$, the best fit of the data. Except at the extremes of the phase function there is very good agreement among the locations of the peaks and troughs, and there is satisfactory agreement among the relative amplitudes of the peaks. Comparing Figures 3 and 5, it is clear that the FFT process greatly improves our ability to interpret noisy data.

Resonance spectra

Although the size and refractive index of a microdroplet can be obtained quite accurately by interpretation of phase functions, resonances provide a much more precise determination of size and refractive index and have the additional advantage that the data are obtained continuously. Resonance data were obtained with a photomultiplier tube (Hamamatsu PMT model 928) mounted on the ring electrode at right angles to the incident laser beam. The output of the PMT and the d.c. potential difference required for particle suspension were recorded with a dual-channel oscillograph.

Figure 6a shows a typical resonance spectrum (intensity vs. time) obtained at $\theta = 90°$ for a dodecanol droplet evaporating in air at room temperature, and Figure 6b shows the theoretical spectrum calculated from Mie theory for $\theta = 90°$ and $m = 1.4395$, the refractive index of dodecanol. The agreement between theory and experiment is excellent and permits us to determine the evaporation rate with high precision. We note a small but very important discrepancy between theory and experiment in the separation between the two resonances in the time increment from 43 to 43.5 min. in the case of the experiment and between $\alpha = 39.8$ and 41.5 in the theory. These experimental resonances are more closely spaced than would be expected from theory. This was due to an explosion of the droplet that was observed to occur at time $t = 43.1$ min. As the droplet evaporated, the surface charge density increased until a critical charge density was reached, the surface ruptured, and a

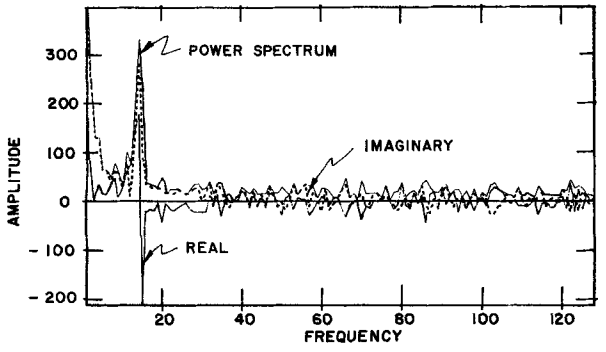

Figure 4. Transformed data corresponding to Figure 3.

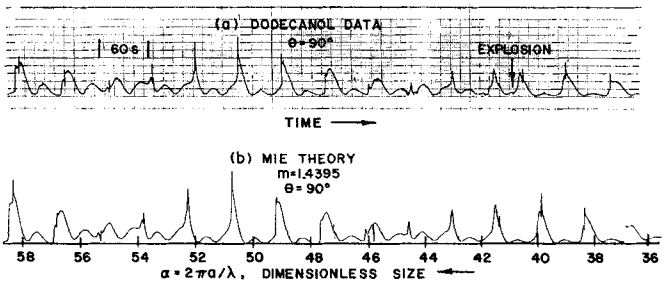

Figure 6. Measured resonance spectrum for dodecanol evaporating in dry air compares with Mie theory.

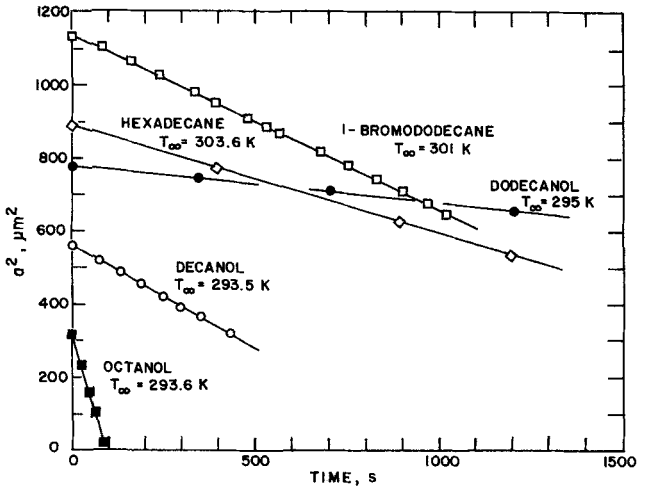

Figure 7. Evaporation rate data for several low-volatility chemicals in dry nitrogen.

small satellite droplet was expelled from the main mass. We shall have more to say about the explosion of droplets below.

Results

Five types of experiments were carried out in this study:

1. Relatively slow evaporation of low vapor pressure single droplets
2. Rapid evaporation of water droplets
3. Slow evaporation of a binary droplet of 1-bromododecane (BDD) and hexadecane (HXD)
4. Rapid evaporation of an aqueous solution of a commercial herbicide
5. Evaporation of surfactant solutions

Single-component Droplets

When the vapor pressure is sufficiently low the surface temperature is very nearly the ambient temperature, as predicted by means of Eq. 5. The dodecanol evaporation data of Figure 6 correspond to such isothermal evaporation, and additional data obtained with decanol, hexadecane, 1-bromododecane, glycerol, and octanol indicate that the surface temperature of the evaporating droplets remained at the gas temperature. Figure 7 shows representative evaporation rate data (a^2 vs. t) obtained by phase function and resonance measurements. The measured slopes, S_{ij}, of the lines can be compared with theoretical values calculated from the knowledge of D_{ij}, p_i^o, ρ_L, and T_∞. The gas phase binary diffusion coefficient can be calculated with reasonable accuracy by a number of methods discussed by Reid et al. (1977), but vapor pressure data at room temperature are either inaccurate or not available for many relatively nonvolatile species. Estimation techniques are not accurate for $p_i^o < 10$ mm Hg (1.33 kPa) (Reid et al., 1977), so calculated values of S_{ij} based on extrapolated values of the vapor pressure can be in great error.

Table 1 compares experimental and predicted values of S_{ij} for a number of low vapor pressure single components studied. The predicted values are based on values of D_{ij} calculated using the semitheoretical method of Fuller et al. (1966) and vapor pressures from the literature cited in the table. The predicted and measured slopes are generally in agreement to within the uncertainty in the vapor pressure. It should be noted that the slopes vary over four orders of magnitude, ranging from 0.00313 $\mu m^2/s$ for dibutyl phthalate at 298.2 K to 4.9 $\mu m^2/s$ for octanol at 293.6 K.

Rapid evaporation leads to interfacial temperatures significantly lower than the surrounding gas temperature, and Figure 8 shows results for water droplets evaporating in dry nitrogen at 283.2 and 293.2 K. Two sets of data for $T_\infty = 283.2$ K are superposed in the figure and show very good reproducibility. The evaporation rates are much lower than those predicted by assuming that the interfacial temperature was at T_∞, shown as dashed lines. For a droplet evaporating with a surface temperature of 293.2 K the slope S_{ij} is calculated to be -790 $\mu m^2/s$, and for 283.2 K the predicted slope is -420 $\mu m^2/s$. Using Eq. 5, however, the interfacial temperatures are calculated to be 277.8 K for $T_\infty = 293.2$ K and 272.7 K for $T_\infty = 283.2$ K, and the predicted slopes are -320 and -220 $\mu m^2/s$, respectively. The initial slopes of the data are in excellent agreement with the predicted values.

Table 1. Comparison of Slopes S_{ij} for Several Low-Volatility Compounds

Chemical	Temp. K	$-S_{ij}$, μm^2 Exp.	$-S_{ij}$, μm^2 Pred.	Ref.
Bromododecane	301	0.478	0.093, 0.71	Stephenson & Malanowski (1987); Pollock & Stevens (1965)
	295	0.338	—	
Decanol	293.5	0.544	0.64	Wilhoit & Zwolinski (1973)
	297	1.01	0.97	
Dibutyl phthalate	298.2	0.00313	0.00394, 0.00423	Ray et al. (1979); Hoyer & Peperle (1958)
Dodecanol	295	0.101	0.098	Smith & Srivastava (1986); Hoyer & Peperle (1958)
	300	0.123	0.141, 0.246	
Glycerol	295	0.0120	0.011, 0.0084	Ross & Heideger (1962); Smith & Srivastava (1986)
	293	0.0079	0.0095, 0.0070	
Hexadecane	295	0.146	0.17, 0.24	Hoyer & Peperle (1958)
Octanol	293.6	4.9	5.74, 7.47	Boublik et al. (1973); Stephenson & Malanowski (1987)

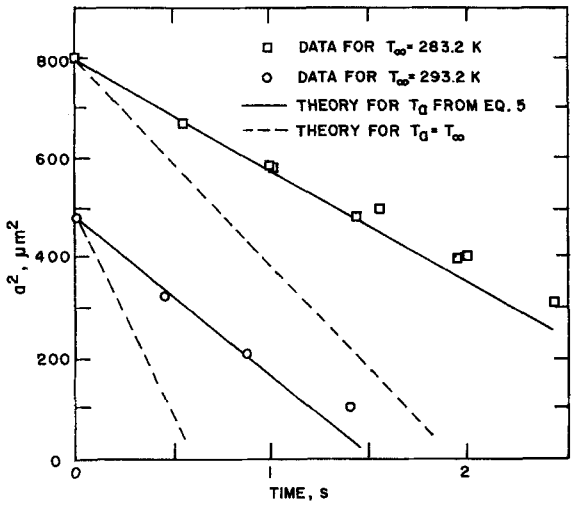

Figure 8. Evaporation rate data for water droplets in dry nitrogen compared with theoretical predictions.

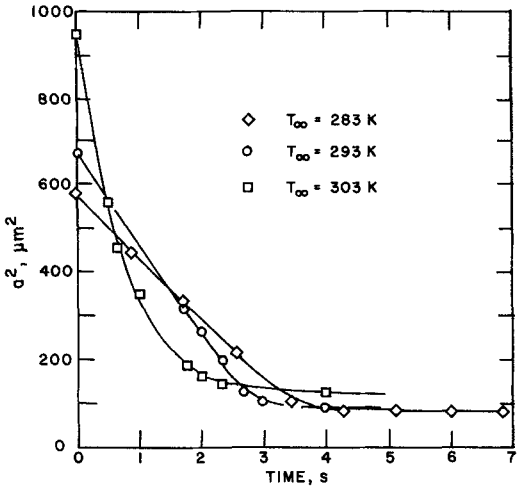

Figure 9. Evaporation rates of droplets of an aqueous solution of hexazinone in dry nitrogen.

Although great care was taken to avoid contamination of the water droplets and triple-distilled water was used, it appears that the experimental slopes decreased with time, probably due to contamination. To examine the effects of contamination we performed experiments with deionized water that had not been triple-distilled; for $T_\infty = 293.2$ K the slope was only $-160\ \mu m^2/s$, which is substantially lower than the value obtained for triple-distilled water. The evaporation process concentrates trace amounts of impurities, and at the end of most experiments a very small particle remained trapped in the laser beam. These remnants showed the irregular light-scattering characteristic of nonuniform solid particles.

We note that for the microdroplet in nitrogen at 283.2 K the predicted droplet temperature is below the freezing point of water. For the short span of these experiments no nucleation occurred, and the droplet remained as subcooled liquid during the entire course of its evaporation.

Multicomponent droplets

The evaporation of aqueous solutions of a low-volatility solute show distinctly different characteristics from pure water droplets. Figure 9 illustrates the behavior of droplets of a commercial agricultural spray. The sizes reported in the figure were obtained from phase function data obtained by the rapid data acquisition technique discussed above. If an agricultural spray is delivered by an airplane, it is undesirable to have so rapid an evaporation rate that the droplets generated by spray nozzles quickly diminish in size to yield a droplet with a low settling velocity. Small droplets will then drift in cross winds before reaching the target. To examine the evaporation characteristics of such materials a dilute aqueous solution of the weed killer hexazinone was introduced into the balance as a droplet of approximately 50 μm dia., and we flowed dry nitrogen through the balance to maintain the humidity of the surrounding gas very nearly zero. The initial evaporation rate was nearly that of water, but as water and hexazinone evaporated, the slope of the a^2 vs. time plot decreased until a relatively low slope was attained, attributable to low-volatility organic chemicals present in the solution. Figure 9 shows that for the temperature range examined most of the volatile components evaporated within 4 s for droplets with initial diameters of 50–60 μm. The size reduction in this time (to 20 μm) would result in a substantial decrease in the terminal velocity of the droplet.

The initial slopes of the data shown in Figure 9 are somewhat lower than those measured for water droplets in dry nitrogen. The measured initial slops are -150, -220, and $-420\ \mu m^2/s$ for $T_\infty = 283.2$, 293.2, and 303.2 K, respectively. It is clear from Figure 9 that a droplet distillation process occurred, for the volatile components were stripped from the solution as evaporation preceeded.

The ability to study rapid droplet evaporation by measuring resonance spectra makes it possible to follow both size and refractive index changes, and we performed a series of experiments to determine if changes in composition can be measured reliably by interpretation of resonance spectra. For this purpose we examined the evaporation of binary droplets of hexadecane (HXD) and 1-bromododecane (BDD). These chemicals have significantly different densities ($\rho_{BDD} = 1{,}039.9$ kg/m^3, $\rho_{HXD} = 773.3$ kg/m^3), different refractive indices ($m_{BDD} = 1.4583$, $m_{HXD} = 1.4345$) and different vapor pressures (at 10 mm Hg [1.33 kPa] BDD boils at 139°C and HXD boils at 149°C). An evaporating droplet is enriched in the less volatile HXD as the evaporation procedes, and the large difference in density makes it possible to follow the composition change from the weight loss as well as by measurement of the resonance spectrum. The refractive index difference between HXD and BDD is sufficient to yield different resonance spectra for the pure components.

Phase functions, resonance spectra, and V_{dc} (to determine the weight) were recorded simultaneously. Figure 10a is a measured resonance spectrum for a droplet that was initially 60 vol. % hexadecane. Interpretation of this spectrum is difficult because the resonances are highly sensitive to refractive index and size, both of which are unknown. Furthermore, there is little unique and readily identifiable structure to the resonances for larger droplets ($\alpha > 100$). For large α, phase functions permit us to determine the size to within about 1%, but they are insensitive to the refractive index. The composition can be estimated from the weight provided that we know the density as a function of composition. Assuming ideal solution behavior, we can write the

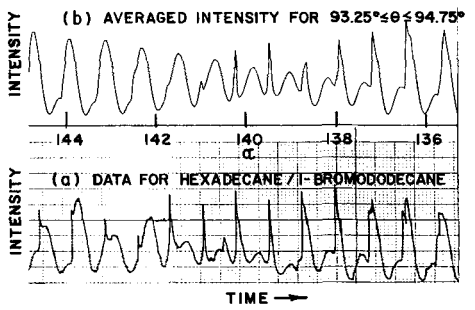

Figure 10. Measured and calculated resonance spectra for a binary solution droplet of hexadecane and 1-bromododecane.

droplet density in terms of the mass fractions, x_i, of the components,

$$\frac{1}{\rho_L} = \frac{x_{HXD}}{\rho_{HXD}} + \frac{x_{BDD}}{\rho_{BDD}} = \frac{1 - x_{BDD}}{\rho_{HXD}} + \frac{x_{BDD}}{\rho_{BDD}} \tag{16}$$

Taking into account the Stokesian drag on the microdroplet, its mass, $m = 4\pi a^3 \rho_L/3$, is related to the d.c. voltage required to suspend the particle by means of the vertical force balance,

$$C_o q V_{dc}/2z_o = 4\pi a^3 \rho_L g/3 - 6\pi a \mu v \tag{17}$$

where C_o and z_o are geometrical constants of the balance, discussed by Davis (1985), q is the charge on the droplet, V_{dc} is the potential difference between the endcaps, g is the gravitational acceleration constant, μ is the viscosity of the gas in the balance, and v is the gas velocity upstream from the droplet. The velocity can be obtained either by calibration (Davis et al., 1987) or by means of the following extrapolation technique. Eliminating ρ_L from Eq. 17 using Eq. 16 and rearranging the resulting equation, we obtain

$$a^2 = \frac{3C_o q}{8\pi g z_o}\left[\frac{x_{BDD}}{\rho_{BDD}} + \frac{(1 - x_{BDD})}{\rho_{HXD}}\right]\left(\frac{V_{dc}}{a} + \frac{12\pi z_o \mu v}{C_o q}\right) \tag{18}$$

Thus, in the limit as $x_{BDD} \to 0$, a plot of a^2 *vs.* V_{dc}/a should yield a straight line with slope $3C_o q/8\pi\rho_{HXD}\, g z_o$ and intercept $9\mu v/2\rho_{HXD}\, g$. Figure 11 is such a plot for a droplet of HXD and BDD near the end of an evaporation experiment. The intercept is 8.489 μm^2, from which we calculate a small convective velocity of 0.818 mm/s.

Now Eq. 18 can be rearranged to give the mass fraction of BDD in terms of the measured values of V_{dc} and a,

$$x_{BDD} = \frac{1}{\left(1 - \dfrac{\rho_{HXD}}{\rho_{BDD}}\right)}\left[1 - \frac{4\pi a^3 g \rho_{HXD}}{3\left(\dfrac{C_o q V_{dc}}{2z_o} + 6\pi a \mu v\right)}\right] \tag{19}$$

If we use a simple mixing rule for the refractive index of the mixture,

$$m = x_{BDD} m_{BDD} + (1 - x_{BDD}) m_{HXD}, \tag{20}$$

the refractive index of the binary droplet can be estimated using x_{BDD} calculated from Eq. 19 in Eq. 20. Using this estimate of m,

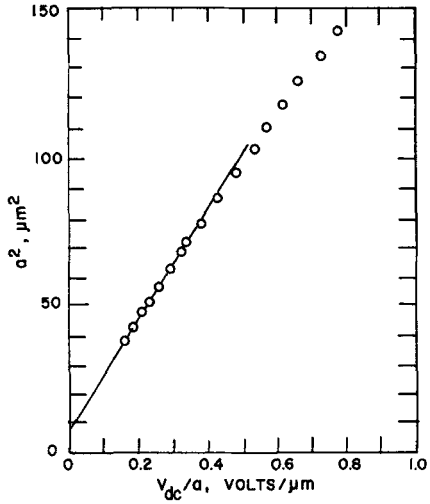

Figure 11. a^2 vs. V_{dc}/a plot based on Eq. 18 used to determine convective velocity in balance chamber.

a calculation of the resonance spectrum for the mixture was made, and further refinements were made by iteration until a best fit was attained. The radii and compositions determined by this procedure are plotted in Figure 12, and the computed best fit for part of the spectrum is shown in Figure 10b. The compositions in Figure 12 that fall below $x_{BDD} = 0$ are, of course, not possible but result from the fact that uncertainty in V_{dc} (about ± 10 mV) produced scatter in the data that was more pronounced near the end of the run when the mass was small. The estimate of composition, using Eq. 19, is very sensitive to V_{dc}, and we estimate that the probable error in composition varies from 0.01 at the beginning of a run to 0.03 at the end.

The agreement between theory and the experimental resonance spectrum is not wholly satisfactory. The light-scattering size deduced from the resonance spectrum agrees well with phase function information, but the correspondence between resonance peaks in the region $139 < \alpha < 143$ is not good.

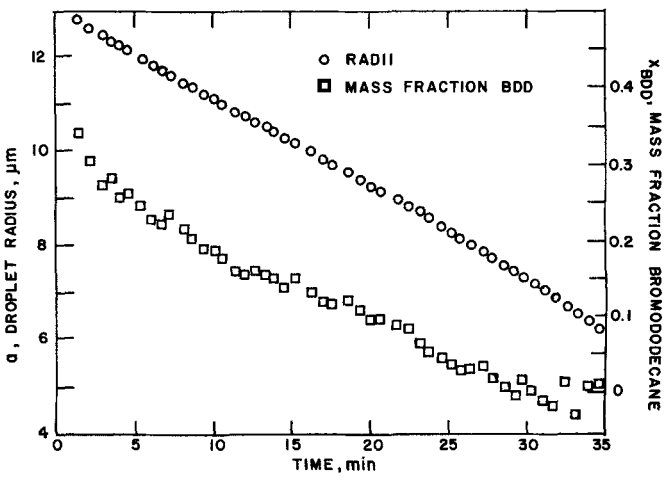

Figure 12. Droplet radius and composition as functions of time for hexadecane-bromododecane binary droplet.

Because of the sensitivity of the resonance spectrum to angle, refractive index, and size it is difficult to conclude which of the uncertainties in these parameters produced the rather poor agreement. The remarkable sensitivity of resonances to size and the agreement between resonance data and phase function data permits us to conclude even with the uncertainty in refractive index that the size can be determined to within 0.1% for a binary system. For a pure component that uncertainty is reduced to 0.01%. Refinements in the experimental technique and methods of analysis by means of pattern recognition formalities are needed to permit us to use resonance spectra alone to determine both size and refractive index, but this is the first attempt at using resonance spectra to obtain both size and composition.

We conclude from the binary component experiments that it is necessary to use phase function data and voltages to interpret the resonance spectra, but the technique shows promise for the study of multicomponent microdroplet mass transfer. We are currently applying Raman and fluorescence spectroscopies (Ward et al., 1987) to determine composition as a function of time, but optical resonance measurements can be made much more rapidly and with considerably less equipment than inelastic scattering measurements, for they do not require expensive monochromators and detectors to determine composition. Inelastic scattering measurements also involve resonance phenomena that make interpretation of spectroscopic data difficult.

Surfactant solution evaporation

The evaporation of a surfactant solution shows quite different mass transfer characteristics compared with the multicomponent results shown in Figures 9 and 12, for the formation of an insoluble monolayer at the droplet surface has a large effect on the evaporation of water from the droplet. To examine these effects we injected single droplets of an aqueous solution of SDS into the electrodynamic balance and recorded phase functions, resonances, and voltages as the droplet evaporated from its initial concentration (10% of the critical micelle concentration) to a liquid crystal state. Typical phase function data are shown in Figure 2, and the resonance spectra for three SDS solution droplets are presented in Figure 13. The initial sizes of the droplets varied, so the lefthand portions of the resonance spectra differ. The two lower spectra show that initially the droplet evaporated so rapidly that the resonances are densely compacted for the chart speed used, but as the experiment proceeded the evaporation rate decreased sharply, and the individual resonances became well defined. The noisy data at the far right of the spectra correspond to the formation of liquid crystals, and once crystals form, the light-scattering data cannot be interpreted to obtain the size.

The resonance spectra are highly reproducible, as indicated by the righthand portions of the three spectra. The slightly different distances between resonances from run to run indicate that the evaporation rates differed somewhat.

Analyses of the phase functions and resonance spectra for SDS solution droplets yield the results shown in Figure 14. The figure indicates that for each run the rapid initial evaporation rate ($S_{ij} = -155\ \mu m^2/s$) was nearly that of water, but after a few seconds the rate changed dramatically and sharply decreased. The evaporation then proceeded with nearly constant S_{ij} ($S_{ij} = -0.667\ \mu m^2/s$) until liquid crystals formed.

It should be noted that during the rapid evaporation period a droplet usually was observed to explode several times, and during the slow evaporation period explosions sometimes occurred. Because of the loss of mass associated with an explosion the rate data must be interpreted with caution. Explosions cause the mass loss rate (or decrease in a^2) to be higher than would be expected for diffusion-controlled evaporation. A careful examination of the resonances of runs 7 and 11 of Figure 13 and the corresponding voltages (not shown) indicates that there was an explosion at the point indicated on the stripchart for run 11, for a resonance is missing. The missing resonance is marked on the stripchart for run 7.

A more detailed analysis of the SDS data and additional surfactant studies for surfactants whose phase diagrams have been established are needed, but it is reasonable to assume that the sudden decrease in evaporation rate was due to the formation of an insoluble layer at the droplet surface. After formation of the interfacial layer the mass transfer became controlled by transport of water through the layer rather than by diffusion of water vapor in the surrounding carrier gas. Continued loss of water would tend to compress the layer, but a droplet explosion would remove some of the surfactant-rich layer, thereby complicating the analysis of the data.

Droplet Explosions

The charge loss associated with the explosion of the dodecanol droplet indicated in Figure 6 and the explosions encountered

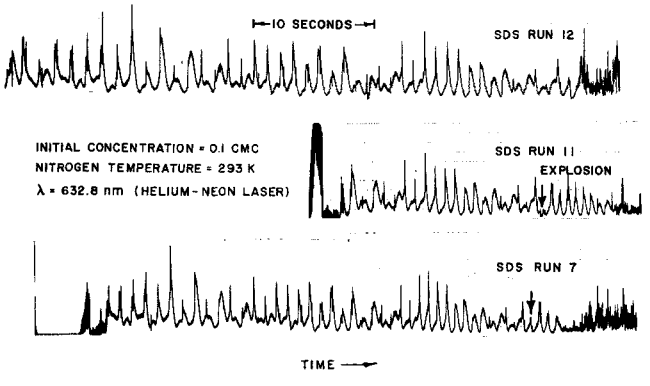

Figure 13. Resonance spectra for three droplets of sodium dodecyl sulfate in water evaporating in dry nitrogen at 293 K.

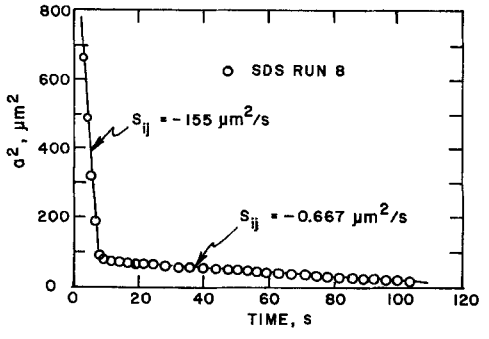

Figure 14. Evaporation rates for a droplet of sodium dodecyl sulfate in water evaporating in dry nitrogen at 293 K.

with surfactant solutions produce a significant change in the charge-to-mass ratio of a microdroplet. This was evidenced by an increase in the d.c. voltage required to suspend the parent droplet. For the dodecanol experiment of Figure 6 the d.c. voltage increased from 0.945 to 0.977 V even though mass was lost because of the explosion.

The charge states before and after the explosion were calculated by applying Eq. 17, using the d.c. voltages and radii measured just before and just after the discontinuity. Although no gas flowed through the balance, there was a slight convective motion within the balance, so it was necessary to determine the convective velocity, v, in Eq. 17. This was accomplished by measuring a and V_{dc} at two times between which the charge was constant but during which a and V_{dc} changed sufficiently to provide an accurate calculation of v, using Eq. 17 to determine the unknowns q and v for the two sets of data. This method yielded a small convective velocity for the dodecanol experiment of -0.0465 cm/s (downward).

The droplet mass prior to the explosion and just after the ejection of the satellite droplet was calculated from the known density and the radii before and after the explosion, which were determined from the resonances. Let a_- be the radius just before the explosion and a_+ be the radius just after the explosion. Measurements of $\alpha = 2\pi a/\lambda$ from Figures 6a and 6b yielded $a_- = 4.362\ \mu$m and $a_+ = 4.304\ \mu$m. The fractional change in the mass, then, is given by $\Delta m/m_- = 1 - (a_+/a_-)^3 = 0.0390$ for the data of Figures 6a and 6b.

Using Eq. 17 and the measured values of V_{dc}, a, and v, the charge q_- prior to the explosion was calculated to be 7.870×10^{-14} Coulomb, which corresponds to 4.943×10^5 elementary charges. After the explosion the charge q_+ was found to be 6.478×10^{-14} Coulomb or 4.069×10^5 elementary charges, and the fractional change in the charge, $\Delta q/q_-$, was 0.177. Thus, the droplet lost 3.9% of its mass and 17.7% of its charge due to disruption of the surface by the electric stress produced by the increased charge density.

One would expect that when the explosion occurred the droplet had reached the Rayleigh limit of charge given by

$$q_R = (16\pi\gamma a^3)^{1/2} \tag{21}$$

where γ is the surface tension of the droplet. If we use Eq. 17 to estimate the surface tension prior to the explosion, based on the measured charge and radius, we obtain $\gamma = 13.3$ mN/m, which is substantially lower than the surface tension of dodecanol (29.14 mN/m). This very surprising result indicates that the droplet exploded when its average surface charge was well below the Rayleigh limit. It is likely, therefore, that a localized perturbation in the surface charge led to the disruption of the surface that expelled 3.9% of the microdroplet mass. It is also possible that local variations in surface tension due to contamination led to explosion before the surface-average charge reached the Rayleigh limit, but dozens of observations and careful measurements of microdroplet explosions that we have made indicate that the explosion usually occurs substantially below the Rayleigh limit of charge.

Conclusions

It has been demonstrated that laser light-scattering methods involving rapid measurement of phase functions and continuous measurement of resonance spectra can be used to study evaporative mass transfer and interfacial phenomena for microdroplets. For the evaporation of relatively nonvolatile single chemicals the theory of isothermal evaporation is in good agreement with data; in fact, the data have sufficient accuracy that they can be used to determine the vapor pressure of the evaporating species. Interfacial temperatures deduced from evaporation experiments with water droplets, which are much more volatile, agree with the quasisteady-state theory of droplet evaporation.

Although resonance measurements can, in principle, be used to determine both the size and refractive index of multicomponent microdroplets, the inversion of resonance data remains an intractable problem. Attempts at matching binary evaporation data with theoretical resonances by forward Lorenz-Mie theory calculations, based on refractive indices estimated from weight loss data, have been only partially successful. For microdroplets with $\alpha < 50$, the resonances are much more unique and identifiable, and optical resonance measurements are easier to interpret. Improvements in the experimental techniques and the method of data analysis are needed for larger droplets, but phase function data provide accurate size information to initiate resonance calculations for matching data.

The observations that microdroplets undergo charge loss by expulsion of a small satellite droplet before the Rayleigh limit is reached were unexpected, but it has been demonstrated that resonance measurements are sufficiently precise to determine the very small size change that occurred. The sudden change in evaporation rate of aqueous solutions of SDS was also surprising, for the transition was sharper than would be expected by the gradual development of an insoluble monolayer. Furthermore, it is not clear what effect the formation of micelles within the droplet has on the light scattering. These issues must be explored in more detail.

Acknowledgment

Acknowledgment is made to the Donors of the Petroleum Research Fund, administered by the American Chemical Society, and to the National Science Foundation for Grant No. CBT-8611779, for their support of this research.

Notation

a = droplet radius, μm
a_n = coefficients, Eq. 1
A_j = amplitude, Eq. 12
B_j = amplitude, Eq. 15
b_n = coefficients, Eq. 1
C_o = geometrical constant of electrodynamic balance
C_{pj} = specific heat of noncondensable gas, J/kg · K
D = distance from middle of photodiode array to center of balance, m
D_{ij} = gas phase diffusivity, m^2/s
g = acceleration of gravity, m/s^2
$h_n^{(2)}$ = Hankel function of the second kind
I_k^* = uncorrected intensity of kth pixel
I_k = corrected intensity of kth pixel
j_n = spherical Bessel function
j_{cutoff} = frequency above which filtering occurred
J_a = mass flux at surface, kg/s · m^2
J_k = intensity vector for equal spacing in θ
k_j = thermal conductivity of noncondensable gas, W/m · K
m = refractive index
M_i = molecular weight of the evaporating species
N = number of pixels in the photodiode array
p_i^o = vapor pressure of the evaporating species, Pa
P = atmospheric pressure, Pa

P_n^1 = associated Legendre function
P_j = power spectrum, Eq. 15
Pe = Peclet number
q = Coulombic charge on microdroplet, C
r = radial coordinate
R = ideal gas constant, J/kmol · K
S_{ij} = slope of a plot of a^2 vs. time, $\mu m^2/s$
t = time, s
T = absolute temperature, K
v = gas velocity, m/s
V_{dc} = d.c. voltage required for microdroplet suspension, V
x = distance of a pixel from center of array, m
x_i = mass fraction
z_o = one-half the minimum distance between endcap electrodes, m

Greek letters

α = light-scattering size
α_T = thermal accommodation coefficient
θ = scattering angle, degrees
λ = wavelength of light, μm
λ_i = heat of vaporization of evaporating species, J/kg
μ = viscosity of noncondensable gas, N · s/m
ρ = liquid density, kg/m^3
γ = surface tension, N/m
ϕ_H = heat transfer correction factor, Eq. 6
ϕ_M = mass transfer correction factor, Eq. 7

Subscripts

a = droplet surface
BDD = bromododecane
HXD = hexadecane
i = evaporating species
j = gas or index
k = index
n = index
o = initial value
∞ = bulk gas

Literature Cited

Arnold, S., and A. B. Pluchino, "IR Spectrum of a Single Aerosol Particle by Photothermal Modulation of Structure Resonances," *Appl. Opt.*, **21,** 4199 (1982).

Arnold, S., E. K. Murphy, and G. Sageev, "Aerosol Particle Molecular Spectroscopy," *Appl. Opt.*, **24,** 1048 (1985).

Ashkin, A., and J. M. Dziedzic, "Observation of Resonances in the Radiation Pressure on Dielectric Spheres," *Phys. Rev. Lett.*, **38,** 1351 (1977).

Barber, P. W., J. F. Owen, and R. K. Chang, "Resonant Scattering for Characterization of Axisymmetric Dielectric Objects," *IEEE Trans. Antennas Prop.*, **IAP-30,** 168 (1982).

Bergland, G. D., "A Rodix-Eight Fast Fourier Transform Subroutine for Real-Valued Series," *IEEE Trans. Audio. Elec.*, **AU-17,** 2 (1969).

Boublik, T., V. Fried, and E. Hala, *The Vapour Pressures of Pure Substances,* 2nd ed., Elsevier, New York (1973).

Chang, R., and E. J. Davis, "Interfacial Conditions and Evaporation Rates of Liquid Droplets," *J. Colloid Interface Sci.*, **47,** 65 (1974).

Chylek, P., J. T. Kiehl, and J. K. W. Ko, "Narrow Resonance Structure in the Mie Scattering Characteristics," *Appl. Opt.*, **17,** 3019 (1978).

Chylek, P., V. Ramaswamy, A. Ashkin, and J. M. Dziedzic, "Simultaneous Determination of Refractive Index and Size of Spherical Dielectric Particles from Light Scattering data," *Appl. Opt.*, **22,** 2302 (1983).

Conwell, P. R., P. W. Barber, and C. K. Rushforth, "Resonant Spectra of Dielectric Spheres," *J. Opt. Soc. Am. A,* **1,** 62 (1984).

Davis, E. J., "Electrodynamic Balance Stability Characteristics and Applications to the Study of Aerocolloidal Particles," *Langmuir,* **1,** 379 (1985).

Davis, E. J., "The Picobalance for Single Microparticle Measurements," *ISA Trans.*, **26,** 1 (1987a).

Davis, E. J., "Single Aerocolloidal Particle Instrumentation and Measurement," *Surface and Colloid Science,* **14,** E. Matijevic, ed., Plenum, New York (1987b).

Davis, E. J., and R. Periasamy, "Light-Scattering and Aerodynamic Size Measurements for Homogeneous and Inhomogeneous Microspheres," *Langmuir,* **1,** 373 (1985).

Davis, E. J., and A. K. Ray, "Single Aerosol Particle Size and Mass Measurements Using an Electrodynamic Balance," *J. Colloid Interface Sci.*, **75,** 566 (1980).

Davis, E. J., S. H. Zhang, J. H. Fulton, and R. Periasamy, "Measurement of the Aerodynamic Drag Force on Single Aerosol Particles," *Aerosol Sci. Tech.* **6,** 273 (1987).

Frey, D. D., and C. J. King, "Effects of Surfactants on Mass Transfer During Spray Drying," *AIChE J.*, **32,** 437 (1986).

Fuller, E. N., P. D. Schettler, and J. C. Giddings, "A New Method for Prediction of Binary Gas-Phase Diffusion Coefficients," *Ind. Eng. Chem.*, **58,** 18 (1966).

Gucker, F. T., and J. J. Egan, "Measurement of the Angular Variation of Light Scattered from Single Aerosol Droplets," *J. Colloid Sci.*, **16,** 68 (1961).

Hoyer, von H., and W. Peperle, "Dampfdruckmessungen an organizchen Substanzen und ihre Sublimationswarmen," *Z. f. Elektrochemie,* **62,** 61 (1958).

Katz, J. L., and P. Mirabel, "Calculation of Supersaturation Profiles in Thermal Diffusion Cloud Chambers," *J. Atmos. Sci.*, **32,** 646 (1975).

Lorenz, L., *Videnskab. Selskab. Skrifter,* **6,** 1 (1890).

Mie, G., "Optics of Turbid Media," *Ann. Physik.*, **25,** 377 (1908).

Pluchino, A. B., "Scattering Photometer for Measuring Single Ice Crystals and Evaporation and Condensation Rates of Liquid Droplets," *J. Opt. Soc. Am.*, **4,** 614 (1987).

Pollock, J. R. A., and R. Stevens, *Dictionary of Organic Compounds,* Oxford Univ. Press, Oxford (1965).

Ray, A. K., E. J. Davis, and P. Ravindran, "Determination of Ultra-low Vapor Pressures by Submicron Droplet Evaporation," *J. Chem. Phys.* **71,** 582 (1979).

Reid, R. C., J. M. Prausnitz, and T. K. Sherwood, *The Properties of Gases and Liquids,* 3rd ed., McGraw-Hill, New York (1977).

Richardson, C. B., R. L. Hightower, and A. L. Pigg, "Optical Measurement of the Evaporation of Sulfuric Acid Droplets," *Appl. Opt.*, **25,** 1226 (1986a).

Richardson, C. B., H.-B. Lin, R. McGraw, and I. N. Tang, "Growth Rate Measurements for Single Suspended Droplets Using the Optical Resonance Method," *Aerosol Sci. Tech.*, **5,** 103 (1986b).

Ross, G. R., W. J. Heideger, "Vapor Pressure of Glycerol" *J. Chem. Eng. Data,* **7,** 505 (1962).

Smith, B. D., and R. Srivastava, *Thermodynamic Data for Pure Compounds,* Elsevier, New York (1986).

Stephenson, R. M., and S. Malanowski, *Handbook of Thermodynamics of Organic Compounds,* Elsevier, New York (1987).

Taflin, D. C., and E. J. Davis, "Mass Transfer from an Aerosol Droplet at Intermediate Peclet Numbers," *Chem. Eng. Commun.*, **55,** 199 (1987).

Tzeng, H.-M., K.F. Wall, M. B. Long, and R. K. Chang, "Evaporation and Condensation Rates of Liquid Droplets Deduced from Structure Resonances in the Fluorescence Spectra," *Opt. Lett.*, **9,** 273 (1984).

Wagner, P. E., "Topics in Current Physics," *Aerosol Microphysics II,* **29,** W. H. Marlow, ed., Springer-Verlag, Berlin (1982).

Ward, T. L., S. H. Zhang, T. Allen, and E. J. Davis, "Photochemical Polymerization of Acrylamide Aerosol Particles," *J. Colloid Interface Sci.*, **118,** 343 (1987).

Wilhoit, R. C., and B. J. Zwolinski, "Physical and Thermodynamic Properties of Aliphatic Alcohols," Nat. Bur. Standards, Washington, DC (1973).

Wuerker, W. F., H. Shelton, and R. V. Langmuir, "Electrodynamic Containment of Charged Particles," *J. Appl. Phys.*, **30,** 342 (1959).

Wyatt, P. J., and D. T. Phillips, "A New Instrument for the Study of Individual Aerosol Particles," *J. Colloid Interface Sci.*, **39,** 125 (1972).

Zhang, S. H., and Davis, E. J., "Mass Transfer from a Single Micro-Droplet to a Gas Flowing at Low Reynolds Number," *Chem. Eng. Commun.*, **50,** 51 (1987).

Manuscript received Dec. 23, 1987, and revision received Mar. 3, 1988.